Chemical Complexity in Local Diffuse and Translucent Clouds: Ubiquitous Linear C 3 H and CH 3 CN, a Detection of HC 3 N and an Upper Limit on the Abundance of CH 2 CN

Harvey S. Liszt, Maryvonne Gerin, Anthony Beasley, Jérôme Pety

GENERATED FEBRUARY 26, 2018
Preprint typeset using LaTeX style AASTeX6 v. 1.0

CHEMICAL COMPLEXITY IN LOCAL DIFFUSE AND TRANSLUCENT CLOUDS: UBIQUITOUS LINEAR-C_3H AND CH_3CN, A DETECTION OF HC_3N AND AN UPPER LIMIT ON THE ABUNDANCE OF CH_2CN

HARVEY LISZT
National Radio Astronomy Observatory
520 Edgemont Road, Charlottesville, VA 22903-2475
hliszt@nrao.edu

MARYVONNE GERIN
LERMA, Observatoire de Paris, PSL Research University,
CNRS, Sorbonne Université, UPMC Université Paris 06,
Ecole Normale Superieure, 75005, Paris, France
gerin@lra.ens.fr

ANTHONY BEASLEY
National Radio Astronomy Observatory
520 Edgemont Road, Charlottesville, VA 22903-2475
tbeasley@nrao.edu

JEROME PETY
Institut de Radioastronomie Millimétrique, 300 Rue de la Piscine, F-38406 Saint Martin d'Hères, France
CNRS, Sorbonne Université, UPMC Université Paris 06,
Ecole Normale Superieure, 75005, Paris, France
pety@iram.fr

ABSTRACT

We present Jansky Very Large Array observations of 20 - 37 GHz absorption lines from nearby Galactic diffuse molecular gas seen against four cosmologically-distant compact radio continuum sources. The main new observational results are that *l*-C_3H and CH_3CN are ubiqitous in the local diffuse molecular interstellar medium at $A_V \lesssim 1$ while HC_3N was seen only toward B0415 at $A_V > 4$ mag. The linear/cyclic ratio is much larger in C_3H than in C_3H_2 and the ratio CH_3CN/HCN is enhanced compared to TMC-1, although not as much as toward the Horsehead Nebula. More consequentially, this work completes a long-term program assessing the abundances of small hydrocarbons (CH, C_2H, linear and cyclic C_3H and C_3H_2, and C_4H and C_4H^-) and the CN-bearing species (CN, HCN, HNC, HC_3N, HC_5N and CH_3CN): their systematics in diffuse molecular gas are presented in detail here. We also observed but did not strongly constrain the abundances of a few oxygen-bearing species, most prominently HNCO. We set limits on the column density of CH_2CN, such that the anion CH_2CN^- is only viable as a carrier of diffuse interstellar bands if the $N(CH_2CN)/N(CH_2CN^-)$ abundance ratio is much smaller in this species than in any others for which the anion has been observed. We argue that complex organic molecules are not present in clouds meeting a reasonable definition of diffuse molecular gas, ie $A_V \lesssim 1$ mag.

Keywords: astrochemistry . ISM: molecules . ISM: clouds. Galaxy

1. INTRODUCTION

The molecular inventory of diffuse interstellar gas is interesting because the unexpectedly high abundances of trace species imply the presence of underlying physical processes that might otherwise remain hidden (Godard et al. 2014). But knowledge of the molecular complement of diffuse molecular gas can be used to advantage even when the underlying

Based on observations obtained with the NRAO Jansky Very Large Array (VLA)

physical processes and observed abundances are only very imperfectly understood:

- Chemistry provides reliable H_2-tracers with well-determined relative abundances from optical astronomy such as OH (X(OH) = N(OH)/N(H_2) = 10^{-7} (Weselak et al. 2009, 2010)) and CH (X(CH) = 3.5×10^{-8} (Sheffer et al. 2008)) as well as HCO^+ that is observed in absorption at 89 GHz with an abundance X(HCO^+) = 3×10^{-9} that can be fixed with respect to both CH and OH (Liszt & Lucas 1996; Liszt et al. 2010; Liszt & Gerin 2016).

- The empirically-determined relative abundance of HCO^+ suffices to explain observations of widely-observed CO in diffuse molecular gas (Liszt et al. 2010) as the product of recombination of HCO^+ with ambient electrons (Glassgold & Langer 1975; Liszt 2007; Visser et al. 2009; Liszt 2017) followed by exchange of carbon isotopes (Watson et al. 1976; Liszt 2017).

- Tallying the inventory of identifiable molecular species sets broad guidelines for attributing practicable carriers of diffuse interstellar bands (DIBs) (Liszt et al. 2012, 2014a). We recently showed that l-C_3H_2 is not sufficiently abundant to serve as the carrier of the DIBs at 4881Å and 5450Å with which it was tentatively identified on the basis of coincidences in laboratory spectra (Maier et al. 2011). Constraining the abundance of another putative DIB-carrier, CH_2CN^- (Cordiner & Sarre 2007), is one aspect of the present work. Knowledge of the abundances of smaller molecules should help in understanding the abundances of broad groups of much larger species like polycyclic aromatic hydrocarbons (PAHs) that may not be individually identifiable.

The molecular inventory of diffuse molecular gas has recently been greatly enlarged using high spectral resolution heterodyne techniques. The HiFi instrument on HERSCHEL observed an extensive inventory of carbon, oxygen and nitrogen hydrides and hydride ions in the sub-mm and THz domains (Gerin et al. 2016), including species long known in optical absorption (CH, CH^+) but also such species as hydrofluoric acid (HF) and the argonium ion ArH^+. CF^+, $c-C_3H$ and HCO were detected in local gas at the IRAM 30m telescope (Liszt et al. 2014b) and CF^+ was subsequently detected in diffuse molecular gas across the galactic disk (Liszt et al. 2015) using NOEMA.

In this work we were motivated to extend the molecular inventory and explore the limits of chemical complexity in diffuse molecular gas, given the recently-developed spectroscopic capabiliies of the enhanced Jansky Very Large Array (VLA). We used the VLA to search at frequencies 20 - 37 GHz for polyatomic molecules whose transitions are most favorably observed in the cm-wave band. We study three chemical families:

- Hydrocarbons. l-C_3H_2 and c-C_3H_2 are the heaviest molecules known in local diffuse molecular gas but they and c-C_3H are as ubiquitous as the lighter hydrocarbons CH and C_2H: by contrast, C_4H has not been detected (Liszt et al. 2012, 2014a). Here we demonstrate the ubiquity and high abundance of l-C_3H and compare the abundances of the linear and cyclic versions of C_3H and C_3H_2. Loison et al. (2017) have recently shown that the relative abundance of the linear and cyclic versions of these molecules represents a competition between formation and isomerization by interaction with atomic hydrogen. The abundance of neutral atomic hydrogen is much higher in diffuse molecular gas, presenting an interesting test of the chemistry. Loison et al. (2017) stress the role of C_3, which is uniquely observable in diffuse molecular gas. Here we show that C_2, also uniquely observable in diffuse molecular gas, is by a slight margin over CH and C_2H the most abundant carbon-bearing molecule after CO: this would not have been possible without a comprehensive survey.

- CN-bearing molecules. The relative abundances of CN, HCN and HNC are very nearly constant in diffuse molecular gas (Liszt & Lucas 2001) but larger CN-bearing species have yet to be detected (Liszt et al. 2008). Here we show that CH_3CN is ubiquitous at A_V = 1 mag, which is quite a surprise given that recent models of the formation of CH_3CN at such moderate extinction predicted an abundance of CH_3CN that is some five orders of magnitude below the observed levels (Majumdar et al. 2014). We also detect HC_3N toward B0415+379 (3C111) at E_{B-V} = 1.6 mag but not toward B2200+420 (BL Lac) at E_{B-V}= 0.33 mag ($E_{B-V} \simeq A_V/3.1$).

- Oxygen-bearing molecules. Previously-detected, lighter oxygen-bearing species include OH, HCO^+, HOC^+, HCO and CO observed at radio frequencies, and H_2O and the many oxygen hydrides and hydride ions observed by HiFi (Gerin et al. 2016). H_2CO, usually thought to form on dust, is known to be ubiquitous in diffuse molecular gas (Nash 1990; Marscher et al. 1993; Liszt et al. 2006) although CH_3OH, which must form on grains, is not detected (Liszt et al. 2008). Here we set limits on an eclectic group of heavier oxygen-bearing species HNCO, HCOOH (formic acid) and H_2COH^+. The systematics of the oxygen-bearing species are not discussed here, owing to the paucity of significant new results.

The plan of this work is as follows. In Section 2 we describe the new observations discussed here and the manner of the presentation of the results. In Sections 3 - 5 we separately discuss the hydrocarbon, CN-bearing and oxygen-bearing species including results for CH, CN, C_2 and C_3 that are observed in optical/UV absorption along sightlines having comparable E_{B-V} and CH to those observed here. Section 6 discusses the viability of CH_2CN^- as a DIB carrier, Section 7 compares our results with those of Thiel et al. (2017) for diffuse clouds observed toward Sgr B2 in the Galactic center and disk and Section 8 is a summary.

2. OBSERVATIONS, CONVENTIONS AND CONVERSION FROM OPTICAL DEPTH TO COLUMN DENSITY

2.1. *Observing and data reduction*

The new observations reported here were taken at the National Radio Observatory's Very Large Array (VLA) on 17 June and 6 July 2013 under proposal 13A-097 while in the C-configuration having angular resolution 25-45 milliarcsec. The data were taken in four scheduling blocks (SB) of 2 hour duration, observing absorption against the continuum targets listed in Table 1 in two orthogonal polarizations. The observing was done with 8 spectral windows having 512 channels of resolution and separation 78 kHz placed opportunistically within the range 20.1 - 22.5 GHz in June (corresponding to velocity resolution 0.104 - 0.115 $\mathrm{km\,s^{-1}}$) and 512 channels of resolution and separation 156 kHz within the range 32.7 - 37.3 GHz in July, corresponding to velocity resolution 0.126 - 0.143 $\mathrm{km\,s^{-1}}$. Spectroscopic properties of the newly-observed spectral lines discussed here are summarized in Table 2.

As in our earlier project discussed in Liszt et al. (2012), two continuum targets and a bandpass calibrator (3C84) were covered in each SB. Considerable time was devoted to reference pointing on each continuum source before it was observed. No absolute amplitude calibration was performed but the fluxes relative to that of the bandbass calibrator 3C 84 ($S_\nu \approx 10 - 16$ Jy) are given in Table 1. In each SB the bandpass calibrator was observed for approximately 20 minutes. The sources were observed for approximately 40 minutes during any one SB execution.

The data were calibrated using very standard techniques in CASA, largely repeating the procedures described in Liszt et al. (2012): Overall the scheme resembles that given in online CASA tutorials for spectral line sources such as TW Hydra with the notable exception that each absorption target, being a phase calibrator, serves as its own phase calibrator. The bandpass calibrator observations were phase-calibrated within each scan sub-interval, followed by construction of an average bandpass solution. This was applied on the fly to complex gain-cal solutions for each continuum target at the sub-scan level, followed by scan-length gain calibration solutions to be applied to each target individually. Once the data were passband- and phase-calibrated in this way they were also fully reduced given the point-like nature of the background targets. For each polarization and baseband, spectra were extracted as vector phase averages over all visibilities, without gridding, mapping or, indeed, more than very minimal manual flagging of bad datapoints. The spectra were produced in CASA's plotms visualizer and exported to drawspec singledish software (Liszt 1997) where spectra in the two polarizations were co-added and very small linear baselines amounting typically to 0.01% of the continuum were removed from each of the basebands.

All velocities discussed here are relative to the kinematic definition of the Local Standard of Rest that is in universal use at radio telescopes.

2.2. *Conversion from integrated optical depth to column density*

Equivalent widths (integrated optical depths) are given in Table 3. For *l*-C_3H the entries are the average of the two lines observed. For CH_3CN the entries for K=0 are the sum of the optical depths of the three K=0 transitions listed in Table 1. The K=0 and K=1 transitions are easily distinguished toward B0415 and B2200 (Figure 4) but not toward B0355, given the complex kinematic structure and modest signal/noise. For B0355 the only quantity given in Table 3 is the integrated optical depth for all kinematic components summed over both K-ladders and the total column density was determined by scaling with respect to the analogous quantity derived toward the sources B2200 and B0415 where the K-ladder structure was resolved..

Default factors needed to convert the observed integrated optical depths (Table 3) to column density (Tables 4-6) are given in the next-to-last column of Table 2: these were computed by assuming rotational excitation in equilibrium with the cosmic microwave background. This is an excellent approximation for strongly-polar diatomics (ie, not CO) and smaller polyatomics having low-J transitions in the mm-wave regime where emission is demonstrably weak, typically a few hundredths of a Kelvin for even optically thick lines (Lucas & Liszt 1996; Liszt & Pety 2016). However, for lower-lying transitions of heavier species observed at cm-wavelengths as in this work, collisional excitation more efficiently redistributes the rotational population out of the lowest states, increasing the numerical factors that should be used to convert observed optical depths to column density.

An upward correction factor due to rotational excitation is tabulated separately as a range in the right-most column of Table 2, corresponding to results for the density range $n(H_2) = 0 - 400\ \mathrm{cm^{-3}}$ that is used in Appendix A. The maximum correction is often below 2 but can be larger when the lowest-lying transition was observed. We have kept the default equivalent width - column density conversion separate from application of the excitation correction, in part because

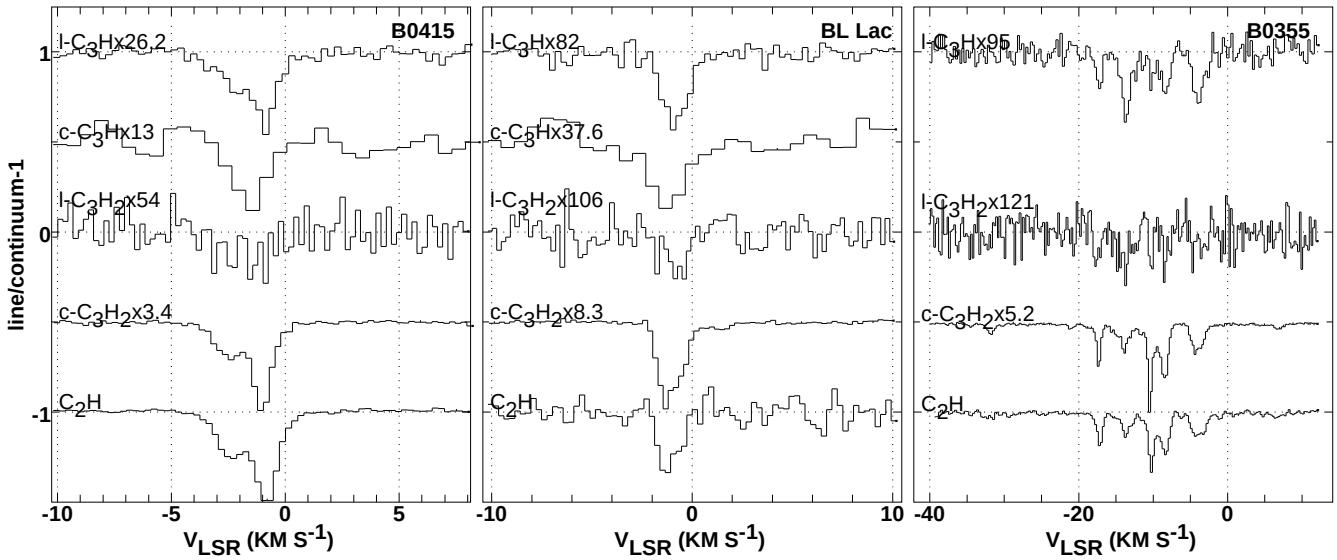

Figure 1. Hydrocarbon line profiles toward B0415+379 ,B2200+420 and B0355+508 , vertically displaced and scaled as indicated. The *l*-C_3H profiles at the top of each panel are new from this work. c-C_3H was not observed toward B0355.

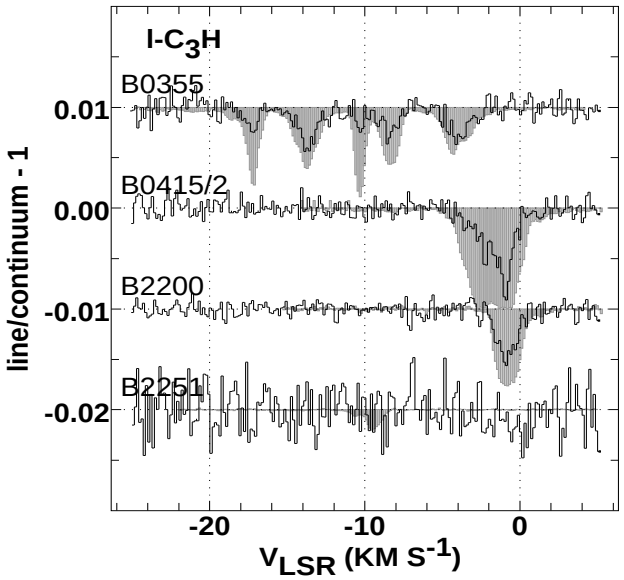

Figure 2. Line profiles of *l*-C_3H for all sources are shown as histrograms compared with profiles of HCO^+ shown shaded in light grey and scaled downward by a factor 100. For B0415 the *l*-C_3H profile has been scaled downward by a factor 2. HCO^+ absorption toward B2251+158 is at -9.6 km s^{-1}.

all of the new observations are unlikely to be characterized by the same density, but the correction should be kept in mind during the discussion and it is noted explicitly in the text as required. Throughout, we have avoided drawing conclusions that seemed unwarranted in the face of this uncertainty.

2.3. *Presentation of results: Figures and tables*

Figure 1 shows results for the newly-detected species *l*-C_3H along with a complement of spectra of previously-observed hydrocarbons having two and three carbons: *c*-C_3H was not observed toward B0355+508 by Liszt et al. (2014b). Figure 2 shows a source-by-source comparison of the newly-detected *l*-C_3H with spectra of HCO^+, the species that shows the fullest extent of molecular absorption in our work. *l*-C_3H is clearly a very ubiquitous species in diffuse molecular gas but with substantial variation in the ratio of the strength of the observed transition to that of J=1-0 HCO^+, as seen by comparing the individual features seen toward B0355. The expected variation of the optical depth-column density conversion factor for *l*-C_3H is approximately 1 - 1.8 for densities in the number density range n(H_2) = 0 – 400 cm^{-3} (Table 2).

Figure 3 compares spectra of the newly-detected CN-bearing species CH_3CN and HC_3N with those of previously-observed nitrogen-bearing species. The -17 km s^{-1} and -11 km s^{-1} components toward B0355+508 that are prominent in the CN-bearing species are just those that are weaker in *l*-C_3H in Figures 1 and 2.

Table 3 gives integrated optical depths for the newly-observed species listed in Table 2 and Tables 4 - 6 give molecular column densities using the integrated optical depths in Table 3, calculated in the limiting case of no collisional excitation above the cosmic microwave background. For B0355+508 the results are listed separately for the kinematic components that are known to exist toward this source in HCO^+. For the other sources, results are shown integrated across the velocity range of the HCO^+ profile.

2.4. *Comparison with other millieu*

The results for diffuse clouds from our work are compared with abundances for the same species determined in other environments in Tables 4 and 5 where detailed references are given, and in passing throughout the text. TMC-1 is the cyanopolyyne peak in the Taurus Dark Cloud, the well-known Horsehead (HH) Nebula hosts a PDR and dense core that are distinguished in the tables. B1b is a complex dark

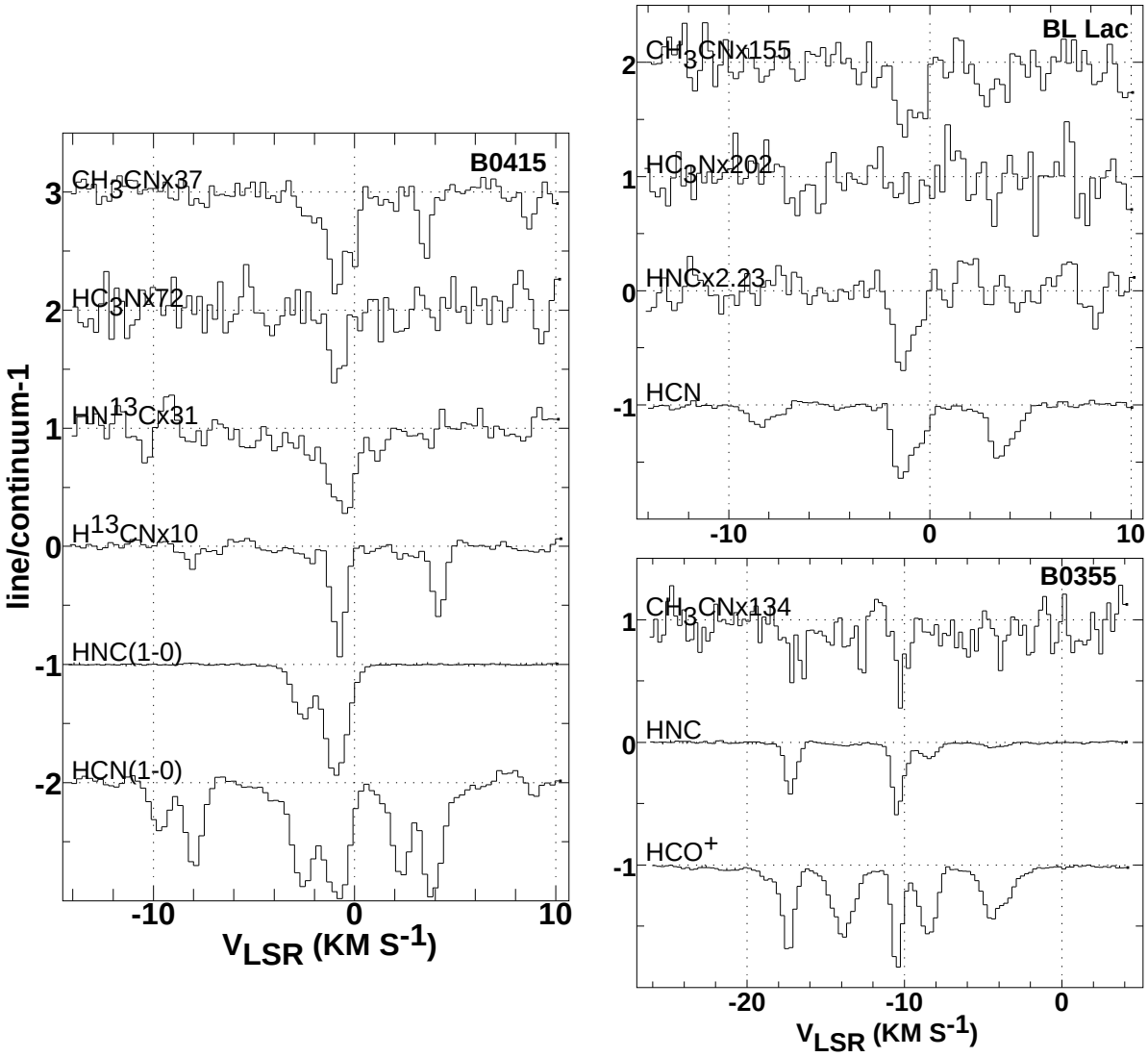

Figure 3. Line profiles of nitrogen-bearing species toward B0415+379, B2200+420 and B0355+508, vertically displaced and scaled as indicated. The HC_3N and CH_3CN profiles are new from this work. The HCN spectrum is not included for B0355 owing to the complexity of the kinematic structure.

cloud core that has higher density and 3-10 times higher column density than TMC-1. Abundances in the Orion Bar are as noted in the references in the tables.

3. THE ABUNDANCES OF SMALL HYDROCARBONS

We previously showed that c-C_3H was ubiquitous in local diffuse molecular gas (Liszt et al. 2014b) and the present work extends this statement to the linear variant l-C_3H. By contrast, C_4H is not detected. Based on the accumulated data shown in Table 4 and previous results for C_4H (Liszt et al. 2012) we summarize the chemistry of small hydrocarbons as follows:

- C_2H is generally the most abundant hydrocarbon. $N(C_2H) \gtrsim N(CH)$ in diffuse molecular gas and dark cloud gas.
- The fractional abundance of C_2H is the same in diffuse molecular gas ($4 \pm 2 \times 10^{-8}$) and toward TMC-1 ($3 - 5 \times 10^{-8}$), but much larger than toward B1b or the Horsehead environments $(0.3 - 1.0) \times 10^{-8}$.
- Adding a third carbon beyond C_2H to form C_3H produces a drop of about a factor 100 in column density in all environments. The drop is larger in diffuse molecular gas ($N(C_2H)/N(C_3H) \approx 200$) than in dark cloud gas or the Horsehead ($N(C_2H)/N(C_3H) \approx 30-70$) if c-C_3H is considered. However, the drop is more nearly equal to 100 in all environments if the comparison is based on l-C_3H.
- The cyclic/linear ratio $N(c\text{-}C_3H)/N(l\text{-}C_3H) \simeq 0.5$ in diffuse molecular gas, comparable to what is observed in the circumstellar envelope around the evolved star IRC+10216 (0.4, see Agúndez et al. (2008)), but very different from the values $N(c\text{-}C_3H)/N(l\text{-}C_3H) \simeq 3 - 10$

in the other environments shown in Table 4.

- The linear variant is much less abundant relative to cyclic in C_3H_2 than in C_3H. The linear/cyclic ratio $N(l\text{-}C_3H_2)/N(c\text{-}C_3H_2) << 1$ in diffuse molecular gas and the Horsehead environments, 1/40 - 1/15, and slightly larger, 1/7-1/6, in dark cloud gas.

- Abundance does not fall uniformly with complexity, C_2H being at least as abundant as CH, and c-C_3H_2 being more abundant than c-C_3H. $N(l\text{-}C_3H)/N(l\text{-}C_3H_2) \approx 1-3$ in all environments, and slightly larger in diffuse molecular gas than otherwise. $N(c\text{-}C_3H)/N(c\text{-}C_3H_2) \approx 1/10$ in diffuse molecular gas, only slightly less than in dark cloud gas (1/6-1/7). The Horsehead environents have ratios nearer unity, $N(c\text{-}C_3H)/N(c\text{-}C_3H_2) \approx 1/2$

- The ratios $N(l\text{-}C_3H)/N(c\text{-}C_3H_2) \approx 0.1-0.2$ observed here (Table 4) are quite comparable to those observed toward Sgr B2 by Corby et al. (2017) in gas of indeterminate E_{B-V}.

- $N(C_4H)/N(C_2H) << 1$ for diffuse molecular gas, smaller than toward TMC-1 where $N(C_4H)/N(C_2H) \approx 0.5$ as we have summarized in Table 4 albeit with large uncertainty in $N(C_4H)$ for TMC-1, see also Liszt et al. (2012). Our measurements of $N(C_4H)$ are insufficiently sensitive to make worthwhile comparisons with C_3H.

The situation is summarized in Figure 5. At left, the molecular column densities are plotted against the far IR dust emission-derived optical reddening equivalents given in Table 1 (Schlegel et al. 1998) and only the total column density toward B0355 can be used; at right the individual kinematic components have been measured for several but not all molecules toward B0355. Also shown in this Figure are values of $N(C_3)$ and $N(C_2)$, using the C_3 column densities of Ádámkovics et al. (2003) and Oka et al. (2003) [1], the C_2 column densities cited in either paper and the CH column densities given by Oka et al. (2003). Inclusion of the results for C_2 and C_3 was motivated by the central role attributed to C_3 in small-hydrocarbon formation in dark clouds by Loison et al. (2017), see their Figure 3. Ironically, $N(C_3)$ is not observable in dark clouds so Loison et al. (2017) did not tabulate calculated values of $N(C_3)$ from their models. Triatomic carbon is observed at THz frequencies in the envelopes and cores of star-forming regions like DR21(OH) with a fractional abundance $X(C_3) \approx 0.6-3.0\times10^{-9}$ (Mookerjea et al. 2012), comparable to what is shown here in Figure 5 [2]. CO aside, C_2 is

[1] The C_3 column densities in common between these references only agree to within a factor two or so

[2] Abundances of C_2H and c-C_3H_2 are also comparable.

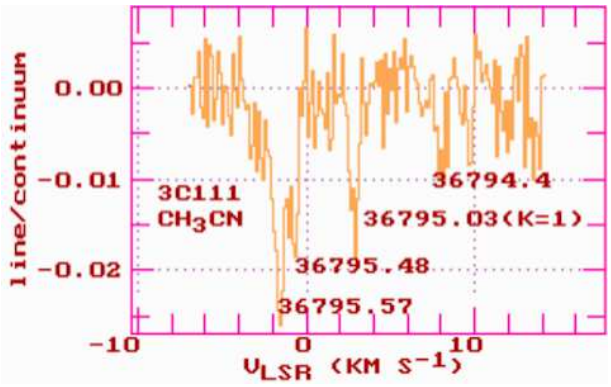

Figure 4. Closeup of CH_3CN K=0 and K=1 lines (Table 1) toward B0415 at 0.127 km s^{-1} spectral resolution.

the most abundant carbon-bearing molecule in diffuse molecular gas, 2-3 times more abundant than either CH or C_2H. The factor 40 drop in abundance between C_2 and C_3 is twice as large as that between C_2H and c-C_3H_2.

Loison et al. (2017) consider in detail the formation of the isomers of the molecular ions that recombine to form C_3H and C_3H_2 along with those of their recombination products, and they took into account the subsequent linear → cyclic isomerization arising from reaction with free atomic hydrogen. They conclude that the comparatively small c-C_3H/l-C_3H ratio ($\approx$ 5) in dark clouds is created during initial formation, either via the reaction of C + C_2H_2 or by dissociative recombination, while the much larger values 30-100 seen in C_3H_2 arise after formation of l-C_3H_2 through linear → cyclic isomerization in reaction with atomic hydrogen.

The c-C_3H_2/l-C_3H_2 ratio in dark clouds decreases with increasing density, which is understood in terms of the smaller atomic hydrogen fraction in denser gas. While this may occur, the much larger atomic hydrogen fraction in diffuse and translucent gas does not lead to yet-larger c-C_3H_2/l-C_3H_2 ratios in our observations, which show quite comparable values to those seen in dark clouds. The inverted ratios c-C_3H/l-C_3H $\approx$ 0.5 in our work have no precedent in dark clouds.

4. THE ABUNDANCE OF POLYYNES AND CN-BEARING SPECIES

- CN itself is the most abundant CN-bearing molecule. $N(CN)/N(H_2) = 3\times10^{-8}$ in diffuse molecular gas and toward TMC-1, or $N(CN)/N(H_2) = 1\times10^{-8}$ toward B1b.

- $N(CN)/N(HCN) \approx 7$ in diffuse molecular gas vs. 1-1.5 in dark cloud gas

- $N(HCN)/N(HNC) \approx 3-6$ in diffuse molecular gas vs. 1 in dark cloud gas, a sign of warmer chemistry in diffuse gas.

- $N(HC_3N)/N(HCN) \leq 0.4$ in diffuse molecular gas comparable to B1b but much less than TMC-1 where $N(HC_3N)/N(HCN) \approx 60$.

- $N(CH_3CN)/N(HCN) \approx 0.015$ in diffuse molecular gas comparable to TMC-1 (0.02) but much greater than B1b (0.002).
- $N(CH_3CN)/N(HC_3N) = 4$ toward B0415, much larger than in dark clouds (1/20 - 1/30), so CH_3CN is enhanced but not by as much as in the Horsehead PDR.
- The large values $N(CH_2CN)/N(CH_3CN) \approx 10$ in dark clouds are not seen in diffuse molecular gas.
- There is no fiducial value for $N(CH_3NC)/N(CH_3CN)$ in dark cloud gas but the best upper limits $N(CH_3NC)/N(CH_3CN) < 0.15 - 0.3$ in diffuse molecular gas are comparable to the abundance ratio $N(CH_3NC)/N(CH_3CN) = 0.15$ seen toward the Horsehead PDR.

The overall situation is summarized in Figure 6 where the optical absorption measurements of N(CN) and $N(C_2)$ cited by Oka et al. (2003) are also included. CN itself is the most abundant CN-bearing molecule, with column densities about 1/3 - 1/2 those of C_2, or comparable to those of CH, at larger E_{B-V} or N(CH). The main result is of course the surprising ubiquity of CH_3CN in diffuse molecular gas, with $X(CH_3CN) = N(CH_3CN)/N(H_2) \approx 0.85 \times 10^{-10}$. That said, there is another surprise in Figure 6: optical CN absorption line data at intermediate E_{B-V} or N(CH) where N(CN) measured in optical absorption is much smaller than N(CN) measured in the radio at the same E_{B-V}. In mm-wave absorption, CN, HCN and HNC appear in nearly fixed proportions (Liszt & Lucas 2001; Ando et al. 2016), with $N(CN)/N(HCN) = 7 \pm 1$. Smaller CN abundances measured in absorption toward early-type stars would suggest photodissociation of CN, especially, as the likely cause. Lamentably, the abilities of optical/UV absorption spectroscopy have not yet allowed detection of species such as HCN in the absorption spectra of stars occulted by diffuse clouds. The optical/UV spectra of HCN and HNC have recently been calculated by Aguado et al. (2017) as part of a computation of the photodissociation rates of both species, showing that the photodissociation rate of HNC is 2.2 times greater. This could account in part for the higher N(HCN)/N(HNC) ratios in diffuse clouds, compared to TMC-1 (see Figure 6 and Table 5).

5. OXYGEN-BEARING SPECIES

Limits on the column densities of isocyanic acid (HNCO), formic acid (HCOOH; found on Earth in ants, bees and nettle plants according to its discoverers Zuckerman et al. (1971)) in the interstellar medium (ISM) and protonated formaldehyde (H_2COH^+) are given in Table 6. HNCO and HCOOH were observed in their lowest transitions, leading to rather large uncertainties in their column densities as noted in Table 1. HNCO can only be said to be less abundant in diffuse molecular gas than in TMC-1 if the excitation is weak in the diffuse molecular gas. There is no fiducial value of the column density of protonated formaldehyde (H_2COH^+) for TMC-1.

6. CH_2CN^- AS A POSSIBLE DIB CARRIER

Cordiner & Sarre (2007) proposed the para-ladder rotational transitions of the anion CH_2CN^- as the carrier of a diffuse interstellar band (DIB) at λ803.7nm. It is this ladder whose lowest rotational transition was observed here in the neutral version of the molecule, CH_2CN. The neutral and its anion have the same symmetry properties, similar rotational structure and roughly comparable permanent dipole moments (3.6 vs. 1.2 Debye, respectively) (Majumdar et al. 2014) so that arguments used in the discussion of the required abundance of the anion should also be used when comparing its column density with that of the neutral observed here. As shown in Table 3, the ratios $N(CH_2CN)/N(CN)$ and $N(CH_2CN)/N(HCN)$ are at least about one order of magnitude smaller in diffuse molecular gas than in dark cloud gas toward TMC-1.

Using Herbig's unpublished data Cordiner & Sarre (2007) determined equivalent widths toward eight stars having reddening $E_{B-V} = 1 - 1.4$ mag, quite comparable to those toward B0355 and B0415 in this work. The results are $< W_\lambda/E_{B-V} >= 0.00220 \pm 0.00064$ nm/mag, or $< N(p\text{-}CH_2CN^-)/E_{B-V} >= 4.025 \times 10^{10}/f$ cm^{-2}/mag where f is the oscillator strength of the λ803.7nm transition. Cordiner & Sarre (2007) hypothesized f=0.5, leading to an implied column density $N(p\text{-}CH_2CN^-) = 1.2 - 1.3 \times 10^{11}$ cm^{-2} toward B0355 and B0415. The upper limits we deduce for $N(p\text{-}CH_2CN)$ toward these sources are somewhat above this, $N(p\text{-}CH_2CN) < 2.5 \times 10^{11}$ cm^{-2} before applying a correction for rotational excitation above that provided by radiative equilibrium with the cosmic microwave background, which is in the range 1-3.

Cordiner & Sarre (2007) showed that two strong spectral features corresponding to absorption out of the ortho-ladder K=1 levels were absent in the optical spectrum, implying that all of the CH_2CN^- resided in the para rotational ladder[3]. To explain this, Cordiner & Sarre (2007) argued that the ortho/para ratio was small because weak collisional excitation in the diffuse molecular ISM would leave all molecules in the lowest possible states, in radiative equilibrium with the cosmic microwave background in all facets of the excitation. Our calculations show that this is a poor assumption for the para-ladder given the large electron fraction in diffuse molecular gas and the large permanent dipole moments of the species in question, but the optical profiles that were integrated to give the equivalent widths naturally include the poorly-resolved rotational sub-structure even if Cordiner & Sarre (2007) did not consider it to be

[3] In fact this could easily be taken to disqualify CH_2CN^- as the carrier.

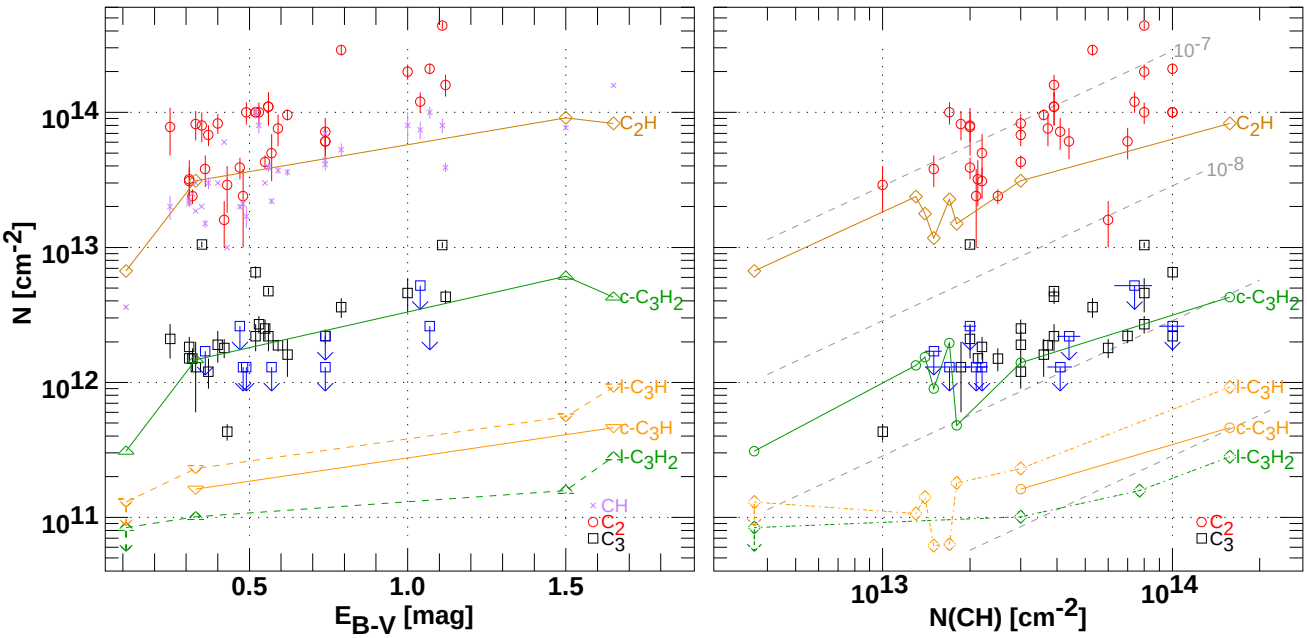

Figure 5. Column densities of C_3, C_2 (Ádámkovics et al. 2003; Oka et al. 2003), CH (Oka et al. 2003) and small hydrocarbons (Table 4). Shown at left are column densities plotted against the IR dust emission-derived optical reddening equivalents (Table 1) for the radio data, or using the stellar reddening for the optical C_2, C_3 and CH data. At right, column densities are plotted against N(CH) using the individual component column densities for the radio data where possible and using N(CH) cited by Oka et al. (2003) for the sightlines observed in optical absorption. Dashed gray lines at right show fractional abundance with respect to H_2 assuming $N(CH)/N(H_2) = 3.5 \times 10^{-8}$.

present. The point is that we are obliged to compare the required column density of p-CH_2CN^- with upper limits for p-$N(CH_2CN)$ that are fully corrected for rotational excitation within the para-rotation ladder even if they weaken our conclusions.

Our limits on $N(p\text{-}CH_2CN)$ are above the required column density of the anion by a factor of a few, 2-6. Under normal circumstances, the large neutral/anion column density ratios > 200 found for other species (Satta et al. 2015) would exclude CH_2CN^- as a possible carrier of the DIB at λ803.7nm. However, Cordiner & Sarre (2007) argued, on the basis of unpublished work by E. Herbst and T. Millar, that the neutral/anion ratio would be exceptionally small, $N(CH_2CN)/N(CH_2CN^-) \approx 1$.

Indeed, small ratios $N(CH_2CN)/N(CH_2CN^-) = 0.25$ - 0.6 were subsequently calculated by Majumdar et al. (2014) who tracked the time evolution of a comprehensive chemical network over a wide range of A_V and n(H). However, the models of Majumdar et al. (2014) also predict $N(CH_2CN^-) = 3.5\times10^7$ cm^{-2} and $N(CH_3CN) = 1.4\times10^5$ cm^{-2} at $A_V = 1$ mag and n(H) = 350 cm^{-3}. These are some 4 orders of magnitude below the required column density of $N(CH_2CN^-)$ but also more than five orders of magnitude below our newly-observed column density of CH_3CN toward B2200+420 (BL Lac) at $A_V = 1$ mag in Table 5. Clearly, the chemistry of CH_2CN^-, and other important anions and molecules possibly linked to DIBs in diffuse molecular gas, must be revisited.

To summarize, our observational upper limit suffices to show that the ratios $N(CH_2CN)/N(CN)$ and $N(CH_2CN)/N(HCN)$ are at least about one order of magnitude smaller in diffuse molecular gas than toward TMC-1. But if it is accepted that the neutral/anion ratio is so much smaller for CH_2CN than for other species, CH_2CN^- might remain a viable carrier of the DIB at λ803.7nm.

7. COMS IN DIFFUSE CLOUDS?

Claims for the presence of various oxygen and nitrogen bearing complex organic molecules (COMS) in diffuse clouds have recently been made on the basis of ALMA observations toward Sgr B2 (Thiel et al. 2017). Some of the column densities derived in that work are shown in Table 7, where we copied results for the three galactic center clouds appearing near 0-velocity (their Table 1) and for the cloud at +27 km s^{-1} assumed to lie in the Scutum arm (their Table 2). For comparison we show results for TMC-1 (A_V = 10-20 mag) and B2200 (A_V = 1 mag), largely as shown in our Tables 5 and 6. For TMC-1 and B2200 we take $N(H^{13}CO^+) = N(HCO^+)/62$, the result obtained for local gas (Lucas & Liszt 1998). The results for $N(CH_3OH)$ are taken from from Liszt et al. (2008) for B2200 and from Ohishi et al. (1992) and Gratier et al. (2016) for TMC-1.

$HCO^+$and c-C_3H_2 are often used as H_2 tracers, for instance with $X(HCO^+) = N(HCO^+)/N(H_2) = 3 \times 10^{-9}$ here, or $X(c\text{-}C_3H_2) = 2.5 \times 10^{-9}$ in the work of Riquelme et al. (2017). As shown in Table 7, the column densities of HCO^+ in the features described as diffuse clouds toward Sgr B2 range from 15 to 200 times larger than toward B2200 and are comparable to or even larger than what is observed in

TMC-1[4]. The c-C_3H_2 column densities seen toward Sgr B2 range up to 12 times that seen toward B2200. Clouds with such comparatively high column densities of the tracers of H_2 cannot also have $A_V \lesssim 1$ mag, the usual meaning of the term "diffuse" (Snow & McCall 2006).

The column densities toward Sgr B2 are 3-20 times larger than toward TMC-1 for CH_3OH, 3-5 times larger than TMC-1 for CH_3CN, and as much as 5 times larger than TMC-1 for HC_3N. They are all several hundred times larger than seen toward B2200. COMS may have been observed toward Sgr B2, but the nature of the host gas remains to be determined.

8. SUMMARY AND DISCUSSION

This work completes several major aspects of a long work program to catalog and systematize the molecular inventory of diffuse molecular gas observed in absorption at radio wavelengths near the Sun and in the wider Galaxy outside the central molecular zone, extending it beyond the very limited complement of mostly-diatomic molecules seen at UV through NIR wavelengths. The case for comparability of the diffuse molecular gas observed in the radio and UV through NIR domains was made in our recent discussions of the suitability of small polar species as carriers of DIBs (Liszt et al. 2012, 2014a) and will not be repeated here, keeping the focus on the observable chemistry of the detected hydrocarbons and CN-bearing species. The oxygen-bearing family of molecules observed at radio wavelengths (OH, CO, HCO, HCO^+, HOC^+, H_2CO and CH_3OH) will be discussed in a forthcoming work that includes recent ALMA observations of HOC^+ and comparisons with existing HERSCHEL observations of H_2O.

The systematics of the small hydrocarbons and CN-bearing species are comprehensively outlined in Sections 3 and 4, respectively. The most abundant species in each family, CH or C_2H and CN, have relative abundances with respect to H_2 that are about equal to each other and the same in diffuse molecular gas and TMC-1, $X(C_2H) = N(C_2H)/N(H_2) = 4 \times 10^{-8}$ and $X(CN) = 3 \times 10^{-8}$ at higher E_{B-V} or $N(H_2)$. However, the most abundant carbon-bearing molecule overall among those considered here (ie, neglecting CO), is C_2 with $X(C_2) = 8 \times 10^{-8}$, 2-3 times more abundant than CH, C_2H or CN. The factor 40 drop in abundance between C_2 and C_3 is twice as large as that between C_2H and c-C_3H_2.

In this work we showed that l-C_3H and CH_3CN are ubiquitous in local diffuse molecular gas and the ratio of CH_3CN to HCN is the same as in TMC-1, $N(CH_3CN)/N(HCN) \approx 0.02$. The relative abundance of c-C_3H is about the same in diffuse molecular gas as in TMC-1 or dark clouds generally Liszt et al. (2014b) but the linear variant is enhanced in diffuse molecular gas: $N(c\text{-}C_3H)/N(l\text{-}C_3H) \approx 0.5$ in diffuse molecular gas, vs 4-10 in the other environments considered in Tables 3-4. The linear variant is much more abundant relative to cyclic in C_3H than in C_3H_2 in all environments.

The c-C_3H_2/l-C_3H_2 ratio in dark clouds decreases with increasing density, which is understood in terms of the smaller atomic hydrogen fraction in denser gas. The much larger atomic hydrogen fraction in diffuse and translucent gas does not lead to yet-larger c-C_3H_2/l-C_3H_2 ratios in our observations, which show quite comparable values to those seen in dark clouds. The inverted ratios c-C_3H/l-$C_3H \approx 0.5$ in our work have no precedent in dark clouds.

In Section 6 we discussed the suitability of CH_2CN^- as a DIB-carrier (Cordiner & Sarre 2007) based on the limits we were able to set on $N(CH_2CN)$. For CH_2CN to be a viable candidate DIB-carrier, the neutral/anion ratio would have to be small, no more than 2-6. Neutral/anion ratios for observed species are typically 200:1 or larger (Satta et al. 2015).

In Section 7 we compared our results with those of Thiel et al. (2017) for three low-velocity clouds and another in the Scutum Arm observed in absorption toward Sgr B2: these observations are the basis of claims for the existence of complex organic molecules (COMS) in diffuse clouds. We noted that column densities of H_2-tracers such as HCO^+ were one - two orders of magnitude higher in that work than those we associate with clouds at $A_V \lesssim 1$ mag locally, and in some cases even larger than those seen in TMC-1. Claims for the presence of COMS in diffuse clouds, material at $A_V \lesssim 1$ mag, must be carefully assessed.

Describing the molecular inventory of diffuse molecular gas is still a work in progress: outstanding undetected hydrocarbons with three carbon atoms include CH_3C_2H and the recently-introduced t-C_3H_2 (Loison et al. 2017) whose microwave spectrum is unknown. t-C_3H_2 could be a common host of unidentified lines given the ubiquity of the other isomers of C_3H_2 in a wide range of astrophysical environments.

Understanding the observed abundance of even some quite small species (CH^+, HCO^+) in diffuse molecular gas requires the addition of new physics into the chemical modelling, as embodied in the work of Godard et al. (2014) and Valdivia et al. (2017). It has further been suggested that the small hydrocarbons observed here should originate in a top-down chemistry after the breakup of much larger species (Guzmán et al. 2015). Observations of polycyclic aromatic hydrocarbons with the James Webb Space Telescope may soon test this idea.

The National Radio Astronomy Observatory is operated by Associated Universities, Inc. under a contract with the National Science Foundation. HL, MG and JP were partially funded by the grant ANR-09-BLAN-0231-01 from the French *Agence Nationale de la Recherche* as part of the SCHISM project (http://schism.ens.fr/) during the early

[4] The very largest disparities might be explained in small part by a smaller $N(HCO^+)/N(H^{13}CO^+)$ ratio if the material near 0-velocity toward Sgr B2 is actually in the central molecular zone.

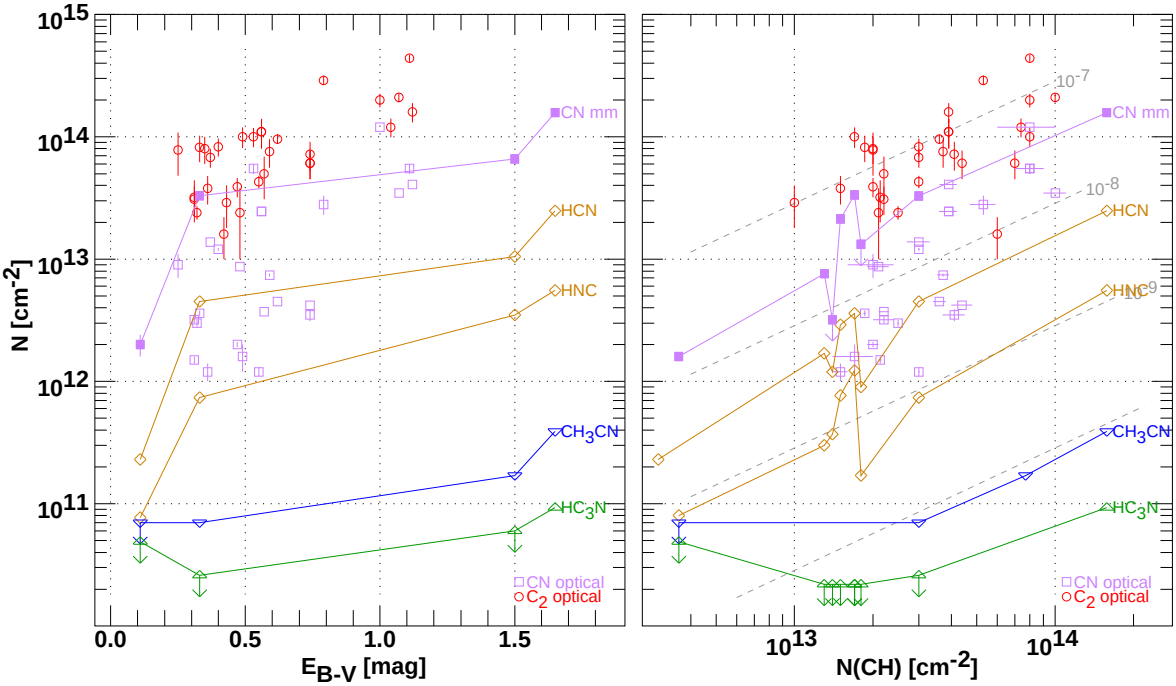

Figure 6. Column densities of C_2 (Ádámkovics et al. 2003; Oka et al. 2003), CH (Oka et al. 2003) and CN-bearing species (Table 5). Shown at left are column densities plotted against the IR dust emission-derived optical reddening equivalents (Table 1) for the radio data, or using the stellar reddening for the optical C_2 and CN data. At right, column densities are plotted against N(CH) using the individual component column densities for the radio data where possible and using N(CH) cited by Oka et al. (2003) for the sightlines observed in optical absorption. Dashed gray lines at right show fractional abundance with respect to H_2 assuming $N(CH)/N(H_2) = 3.5 \times 10^{-8}$.

Table 1. Continuum target and sightline properties

Target	aka	l	b	E_{B-V}[a]	flux[b]
		o	o	mag	%
B0355+508	NRAO150	150.38	-1.60	1.50	28,29
B0415+379	3C111	161.67	-8.82	1.65	8,10
B2200+420	BL Lac	92.59	-10.44	0.33	28,31
B2251+158	3C454.3	86.11	-38.18	0.11	16,21

[a]from Schlegel et al. (1998)
[b] entries are 21 GHz and 36 GHz fluxes as percentages of 3C84 ($S_\nu \approx 16, 10$ Jy)

phases of this work. The work of MG and JP was supported by the CNRS program "Physique et Chimie du Milieu Interstellaire"(PCMI). The work of MG and JP was supported by the Programme National "Physique et Chimie du Milieu Interstellaire" (PCMI) of CNRS/INSU with INC/INP co-funded by CEA and CNES.

We thank the Alexandre Faure for providing excitation rates for CH_3CN and we thank the anonymous referee for a variety of remarks that led to improvements in the manuscript.

Facility: VLA

Software: DRAWSPEC (Liszt 1997), CASA (McMullin et al. 2007)

APPENDIX

A. ROTATIONAL EXCITATION

For the low-lying transitions of heavier species observed in this work, collisional excitation redistributes the rotational population out of the lowest states, increasing the numerical factors that should be used to convert observed optical depths to column density. Collisions with electrons greatly dominate the excitation in diffuse molecular gas where the CO abundance is small and C^+ is the dominant carrier of carbon leading to an electron fraction $n(e)/n(H) \gtrsim 1.4 \times 10^{-4}$ (Sofia et al. 2004). Excitation rates for collisions with He and H_2 play a smaller role and have not been calculated for most of the species discussed here but we included H_2 excitation of HC_3N (Faure et al. 2016) and excitation of CH_3CN by He and H_2 (Faure, private communication). Electron excitation is considered here as in Liszt (2012), using separate closed-form approximations for molecular ions and neutrals.

The excitation rate coefficients and our excitation calculations are not hyperfine-resolved and are just recalculations of the rotational partition function. Results of the excitation calculations are illustrated in Figure A.1 for hydrocarbons and CN-bearing species and in Figure A.2 for the oxygen-bearing species. The normalization on the vertical axis is such that the integrated optical

Table 2. Species and transitions observed and column density-optical depth conversion factors at $T_{ex}=T_{CMB}$

Species	ortho/para/other	transition	frequency MHz	$\log(A_{kj}\ s^{-1})$[a]	$N(X)/\int \tau dv$[b] $cm^{-2}\ (km\ s^{-1})^{-1}$	Correction[e]
l-C_3H	$l = f$	J=3/2-1/2,Ω=1/2,F=2-1	32627.30	-5.89	2.82×10^{13}	1-1.8
l-C_3H	$l = e$	J=3/2-1/2,Ω=1/2,F=2-1	32660.65	-5.89	2.82×10^{13}	1-1.8
HC_3N[c]		J=4-3	36292.33	-5.49	1.09×10^{13}	1-1.6
CH_3CN	E	2(0)-1(0) F=3-2	36795.57	-5.45	1.27×10^{13}	1-1.7
CH_3CN	E	2(0)-1(0) F=2-1	36795.48	-5.57	2.38×10^{13}	1-1.7
CH_3CN	E	2(0)-1(0) F=1-0	36794.42	-5.70	5.47×10^{13}	1-1.7
CH_3CN	A	2(1)-1(1) F=1-0	36795.03	-5.57	1.19×10^{13}	1-1.7
CH_3NC	E	1(0)-0(0)	20105.75	-6.32	1.07×10^{13}	1-4.5
CH_2CN[d]	p	$1_{01} - 0_{00}$	20119.61	-6.41	7.73×10^{13}	1-3.5
HNCO		1(0,1)-0(0,0) F=2-1	21981.46	-6.98	6.39×10^{13}	1-6
HCOOH	t	1(0,1)-0(0,0)	22471.18	-7.07	6.80×10^{13}	1-7
H_2COH^+		2(0,2)-1(1,1)	36299.95	-6.51	5.61×10^{13}	1-1.6

[a] www.splatalogue.net
[b] for the observed ortho or para version only, assuming rotational excitation in equilibrium with the cosmic microwave background
[c] 96% of the integrated intensity is in an unresolved blend
[d] J=3/2-1/2,F_1=5/2-3/2,F=7/2-5/2. Spectroscopy from Irvine et al. (1988) and Ohishi & Kaifu (1998)
[e] See Figures A1-A2

Table 3. Integrated optical depths (EW) for newly-observed species [a]

Target	vel	EW	EW	EW	EW	EW	EW	EW	EW	EW
	$km\ s^{-1}$	$m\ s^{-1}$	$m\ s^{-1}$	$m\ s^{-1}$	$m\ s^{-1}$	$m\ s^{-1}$	$m\ s^{-1}$	$m\ s^{-1}$	$m\ s^{-1}$	$m\ s^{-1}$
		l-C_3H	HC_3N	CH_3CN[b]	CH_3CN[c]	CH_3NC	CH_2CN	HNCO	HCOOH	H_2COH^+
B0355+508	-17	2.20(0.56)	< 2.0			< 1.71	< 1.90	<2.10	<2.21	<3.63
	-14	6.40(0.64)								
	-10	2.22(0.48)								
	-8	3.56(0.56)								
	-4	5.00(0.70)								
	all	19.3(0.13)	< 5.5	23.0(3.0)[d]		< 4.47	<3.24	<4.86	<4.80	<7.98
B0415+379		32.8(1.75)	8.5(1.9)	42.4(3.2)	9.7(1.8)	< 4.16	<3.15	<4.62	<4.62	<9.30
B2200+420		8.16(0.4)	< 2.55	7.4(1.2)	2.3(0.6)	< 1.92	<1.68	<1.65	<1.95	<2.94
B2251+158		< 4.5	< 4.5	<7.1		< 4.92	<3.90			<7.31

[a] all upper limits are 3σ
[b] The sum of the three observed K=0 lines
[c] K=1
[d] K=0 and K=1 are not distinguishable, this is their sum

depth of the transition in question corresponds to a total column density $N = 10^{11}\ cm^{-2}$ (shown in each panel) but it is only the extent of the variation across the horizontal axis that matters. The default optical depth-column density conversion factor given in the next-to-last column of Table 2 corresponds to zero density at the left and the maximum correction corresponds to the amount by which the curves have fallen at $n(H_2) = 400\ cm^{-3}$. The very lowest-lying transitions are quite sensitive to density variations while those lying higher may be nearly unaffected. The excitation, being dominated by electrons, is only weakly sensitive to the kinetic temperature as shown in Figures A.1 and A.2 where the calculations have been carried out for kinetic temperatures of 20, 40 and 60 K: the different curves at these tempertures often overlap to the point that they are indistinguishable.

REFERENCES

Ádámkovics, M., Blake, G. A., & McCall, B. J. 2003, ApJ, 595, 235

Aguado, A., Roncero, O., Zanchet, A., Agúndez, M., & Cernicharo, J. 2017, ApJ, 838, 33

Table 4. Column densities for hydrocarbons

Target	v	$N(H_2)^1$	$N(CH)^2$	$N(C_2H)^a$	$N(c\text{-}C_3H_2)^b$	$N(l\text{-}C_3H_2)^c$	$N(C_4H)^m$	$N(c\text{-}C_3H)^d$	$N(l\text{-}C_3H)$
	km s^{-1}	10^{20} cm^{-2}	10^{13} cm^{-2}	10^{13} cm^{-2}	10^{12} cm^{-2}	10^{11} cm^{-2}	10^{13} cm^{-2}	10^{11} cm^{-2}	10^{11} cm^{-2}
B0355	-17	4.3	1.5	1.17	0.90				0.62(0.16)
	-14	5.0	1.8	1.50	0.48				1.81(0.18)
	-10	4.8	1.7	2.27	1.96				0.63(0..14)
	-8	3.8	1.3	2.38	1.34				1.07(0.16)
	-4	4.0	1.4	1.78	1.54				1.41 (0.20)
	-all	22	7.7	9.10	6.11	1.58	<1		5.56(0.34)
B0415		45	15.8	8.29	4.28	2.81	< 2.3	4.63(0.18)	9.24(0.49)
B2200		8.7	3.0	3.11	1.47	1.01	< 0.4	1.62(0.05)	2.30(0.13)
B2251^e		1.0	0.36	0.67	0.31	< 0.84	< 0.3		< 1.3
TMC-1/10^f		10	2	5-10	10		2	6	5
TMC-1/10^g		”			2	0.6	0.3-9	18	6
TMC-1/10^h		”		6	12	2		10	1
TMC-1/10^i		”		2	6	2		10	1
consensus		10-20^l	2	5	6	1	2	9	2
B1b/10^j		$\gtrsim$ 60			2	0.6		6	1
HH PDR/10^k		19		1-2	0.5-0.8	0.5-1.5		2-7	0.6 - 1.8
HH core/10^k		32		< 1	0.3-0.4	0.1-0.3		0.8-2.3	0.1-0.4
Orion Bar/10^n		30		4	1.3	0.4	0.4	2	0.6

[1] $N(H_2) = N(HCO^+)/3 \times 10^{-9}$ for sources observed in this work
[2] $N(CH) = N(H_2) \times 3.5 \times 10^{-8}$ for sources observed in this work
[a] $N(C_2H)$ from Lucas & Liszt (2000)
[b] $N(c\text{-}C_3H_2) = (4/3) \times N(o\text{-}c\text{-}C_3H_2)$ from Liszt et al. (2012)
[c] $N(l\text{-}C_3H_2) = 4 \times N(p\text{-}l\text{-}C_3H_2)$ from Liszt et al. (2012)
[d] $N(c\text{-}C_3H)$ from Liszt et al. (2014b)
[e] upper limits are 3σ
[f] Ohishi et al. (1992) whose tables must be interpreted with $N(H_2) = 10^{22}$ cm^{-2}
[g] Gratier et al. (2016)
[h] Loison et al. (2017) except C_2H from Sakai et al. (2010)
[i] Fossé et al. (2001)
[j] Loison et al. (2017) and Daniel et al. (2013)
[k] Horsehead (HH nebula values from Guzmán et al. (2015)
[l] $N(H_2) \geq 2 \times 10^{22}$ cm^{-2} beam-averaged on 1′ scales is given by Fehér et al. (2016)
[m] Results for C_4H from Liszt et al. (2012)
[n] Cuadrado et al. (2015), Table 6

Agúndez, M., Cernicharo, J., Pardo, J. R., et al. 2008, Astrophys. Space. Sci., 313, 229
Ando, R., Kohno, K., Tamura, Y., et al. 2016, Publ. Astron. Soc. Jpn., 68, 6
Corby, J., McGuire, B., Herbst, E., & Remijan, A. 2017, ArXiv e-prints, arXiv:1708.03432
Cordiner, M. A., & Sarre, P. J. 2007, A&A, 472, 537
Cuadrado, S., Goicoechea, J. R., Cernicharo, J., et al. 2017, A&A, 603, A124
Cuadrado, S., Goicoechea, J. R., Pilleri, P., et al. 2015, A&A, 575, A82
Daniel, F., Gerin, M., Roueff, E., et al. 2013, A&A, 560, A3
Faure, A., Lique, F., & Wiesenfeld, L. 2016, Mon. Not. R. Astron. Soc., 460, 2103
Fehér, O., Tóth, L. V., Ward-Thompson, D., et al. 2016, A&A, 590, A75
Fossé, D., Cernicharo, J., Gerin, M., & Cox, P. 2001, ApJ, 552, 168
Gerin, M., Neufeld, D. A., & Goicoechea, J. R. 2016, Ann. Rev. Astrophys. Astron., 54, 181
Glassgold, A. E., & Langer, W. D. 1975, ApJ, 197, 347
Godard, B., Falgarone, E., & Pineau des Forêts, G. 2014, A&A, 570, A27
Gratier, P., Majumdar, L., Ohishi, M., et al. 2016, Astrophys. J., Suppl. Ser., 225, 25
Gratier, P., Pety, J., Guzmán, V., et al. 2013, A&A, 557, A101
Guzmán, V. V., Pety, J., Goicoechea, J. R., et al. 2015, ApJ, 800, L33
Irvine, W. M., Friberg, P., Hjalmarson, A., et al. 1988, ApJ, 334, L107
Liszt, H., & Lucas, R. 2001, A&A, 370, 576
Liszt, H., Lucas, R., & Pety, J. 2006, A&A, 448, 253
Liszt, H., Lucas, R., Pety, J., & Gerin, M. 2014a, in IAU Symposium, Vol. 297, The Diffuse Interstellar Bands, ed. J. Cami & N. L. J. Cox, 163–172
Liszt, H., Sonnentrucker, P., Cordiner, M., & Gerin, M. 2012, ApJ, 753, L28
Liszt, H. S. 1997, in Astronomical Society of the Pacific Conference Series, Vol. 125, Astronomical Data Analysis Software and Systems VI, ed. G. Hunt & H. Payne, 3
Liszt, H. S. 2007, A&A, 476, 291
—. 2012, A&A, 538, A27
—. 2017, ApJ, 835, 138
Liszt, H. S., & Gerin, M. 2016, A&A, 585, A80
Liszt, H. S., Guzmán, V. V., Pety, J., et al. 2015, A&A, 579, A12
Liszt, H. S., & Lucas, R. 1996, A&A, 314, 917
Liszt, H. S., & Pety, J. 2016, ApJ, 823, 124
Liszt, H. S., Pety, J., Gerin, M., & Lucas, R. 2014b, A&A, 564, A64

Table 5. Column densities for CN-family molecules[a]

Target	v	N(H_2)	N(CN)[b]	N(HCN)[b]	N(HNC)[b]	N(HC_3N)	N(CH_3CN)[c]	N(CH_3NC)	N(CH_2CN)
	km s^{-1}	10^{20} cm^{-2}	10^{13} cm^{-2}	10^{13} cm^{-2}	10^{13} cm^{-2}	10^{11} cm^{-2}	10^{11} cm^{-2}	10^{11} cm^{-2}	10^{11} cm^{-2}
B0355	-17	4.3	2.13	0.29	0.077	<0.22		< 0.18	< 1.5
	-14	5.0	<0.32	0.09	0.017				
	-10	4.8	3.35	0.36	0.123				
	-8	3.8	0.76	0.17	0.030				
	-4	4.0	<0.32	0.12	0.037				
	-all	22	6.6	1.05	0.28	<0.60	1.7(0.2)	<0.37	< 2.5
B0415		45	15.78	2.480	0.554	0.93(0.21)	3.9(0.3)	<0.44	< 2.4
B2200		8.7	3.29	0.450	0.074	<0.26	0.7(0.1)	<0.20	< 1.3
B2251		1.0	0.20	0.023	0.008	<0.49	<0.7	<0.52	< 3.0
TMC-1/10[d]		10	3	2	2	60	10		50
TMC-1/10[e]						234	4		38
consensus		10 – 20[i]	3	2	2	120	6		44
B1b/10[g]		$\gtrsim$ 60	6	5	2	2	0.1		
HH-PDR[h]						2.5	100	15	
HH-core[h]						5	5	<5	
Orion Bar[j]/10		30	2.5	0.34	0.4	3	7		

[a] all upper limits are 3σ
[b] N(CN), N(HCN) and N(HNC) from Liszt & Lucas (2001)
[c] Sum of N(CH_3CN) K=0 and K=1
[d] Ohishi et al. (1992) whose tables must be interpreted with N(H_2) = 10^{22} cm^{-2}
[e] Gratier et al. (2016)
[g] Loison et al. (2017) and Daniel et al. (2013)
[h] Horsehead nebula values from Pety et al. (2012), Gratier et al. (2013) and Guzmán et al. (2015)
[i] N(H_2) $\geq 2 \times 10^{22}$ cm^{-2} beam-averaged on 1′ scales is given by Fehér et al. (2016)
[j] Cuadrado et al. (2017)

Table 6. Column densities for oxygen-bearing molecules[a]

Target	v	N(H_2)	N(HNCO)	HCOOH	H_2COH^+
	km s^{-1}	10^{20} cm^{-2}	10^{11} cm^{-2}	10^{11} cm^{-2}	10^{11} cm^{-2}
B0355	-17	4.3	<1.3	<1.5	<2.0
	-14	5.0			
	-10	4.8			
	-8	3.8			
	-4	3.8			
	-all	22	<3.1	<3.2	<4.5
B0415		45	<3.0	<3.1	<5.2
B2200		8.7	<1.1	<1.3	<1.6
B2251		1.0			<4.1
TMC-1/10[d]		10	2	< 2	
TMC-1/10[e]			11		
consensus		10-20[f]	4.7	< 2	

[d] TMC-1 values from Ohishi et al. (1992)
[e] TMC-1 values from Gratier et al. (2016)
[f] N(H_2) $\geq 2 \times 10^{22}$ cm^{-2} beam-averaged on 1′ scales according to Fehér et al. (2016)

Liszt, H. S., Pety, J., & Lucas, R. 2008, A&A, 486, 493
—. 2010, A&A, 518, A45
Loison, J.-C., Agúndez, M., Wakelam, V., et al. 2017, Mon. Not. R. Astron. Soc., 470, 4075
Lucas, R., & Liszt, H. 1998, A&A, 337, 246
Lucas, R., & Liszt, H. S. 1996, A&A, 307, 237
—. 2000, A&A, 355, 327
Maier, J. P., Walker, G. A. H., Bohlender, D. A., et al. 2011, ApJ, 726, 41
Majumdar, L., Das, A., & Chakrabarti, S. K. 2014, A&A, 562, A56
Marscher, A. P., Moore, E. M., & Bania, T. M. 1993, ApJ, 419, L101
Mookerjea, B., Hassel, G. E., Gerin, M., et al. 2012, A&A, 546, A75
Nash, A. G. 1990, Astrophys. J., Suppl. Ser., 72, 303
Ohishi, M., Irvine, W., & Kaifu, N. 1992, in Astrochemistry of cosmic phenomena: proceedings of the 150th Symposium of the International Astronomical Union, held at Campos do Jordao, Sao Paulo, Brazil, August 5-9, 1991. Dordrecht: Kluwer, ed. P. D. Singh, 171–172
Ohishi, M., & Kaifu, N. 1998, Faraday Discussions, 109, 205
Oka, T., Thorburn, J. A., McCall, B. J., et al. 2003, ApJ, 582, 823
Pety, J., Gratier, P., Guzmán, V., et al. 2012, A&A, 548, A68
Riquelme, D., Bronfman, L., Mauersberger, R., et al. 2017, ArXiv e-prints, arXiv:1709.02464
Sakai, N., Saruwatari, O., Sakai, T., Takano, S., & Yamamoto, S. 2010, A&A, 512, A31+
Satta, M., Gianturco, F. A., Carelli, F., & Wester, R. 2015, ApJ, 799, 228
Schlegel, D. J., Finkbeiner, D. P., & Davis, M. 1998, ApJ, 500, 525
Sheffer, Y., Rogers, M., Federman, S. R., et al. 2008, ApJ, 687, 1075
Snow, T. P., & McCall, B. J. 2006, Ann. Rev. Astrophys. Astron., 44, 367
Sofia, U. J., Lauroesch, J. T., Meyer, D. M., & Cartledge, S. I. B. 2004, ApJ, 605, 272
Thiel, V., Belloche, A., Menten, K. M., Garrod, R. T., & Müller, H. S. P. 2017, A&A, 605, L6
Valdivia, V., Godard, B., Hennebelle, P., et al. 2017, A&A, 600, A114

Table 7. Comparison with Galactic Center and Scutum Arm diffuse clouds of Thiel et al. (2017)

Species	TMC-1	B2200	GC 1	GC 2	GC 3	Scutum
	cm^{-2}	cm^{-2}	cm^{-2}	cm^{-2}	cm^{-2}	cm^{-2}
$H^{13}CO^+$	1.3×10^{12} [a]	0.042×10^{12} [a]	1.5×10^{12}	8×10^{12}	4×10^{12}	0.6×10^{12}
c-C_3H_2	2.0×10^{13}	0.150×10^{13}	0.5×10^{13}	2×10^{13}	1×10^{13}	0.8×10^{13}
CH_3OH	0.2×10^{14}	$< 0.005\times10^{14}$	4×10^{14}	4×10^{14}	2×10^{14}	0.6×10^{14}
CH_3CN	0.4×10^{13}	0.007×10^{13}	1×10^{13}	2×10^{13}	$< 6\times10^{13}$	1.4×10^{13}
HC_3N	13×10^{13}	$< 0.004\times10^{13}$	$< 3\times10^{13}$	60×10^{13}	$< 3\times10^{13}$	$< 2.5\times10^{13}$

[a] $N(H^{13}CO^+) = N(HCO^+)/62$

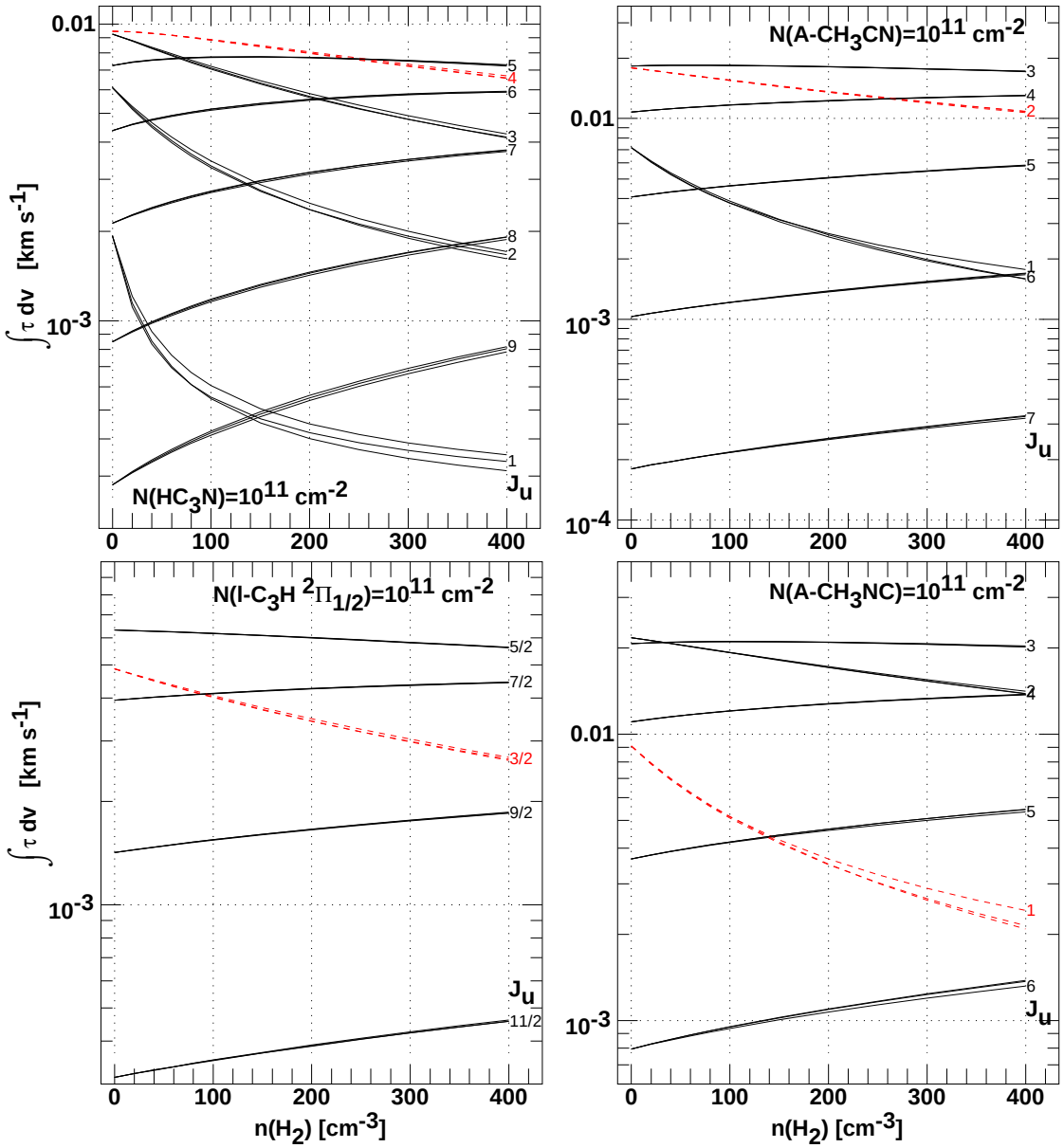

Figure A1. Integrated optical depth for rotational transitions of four molecules observed in the course of this work, assuming a column density of 10^{11} cm^{-2} in each case. The plots show the integrated optical depth of transitions whose upper-level quantum number is shown at the right of each series of three curves. The three curves for each transition correspond to calculations at kinetic temperatures of 20, 40 and 60 K and are often indistinguishable. The excitation calculations include H_2 and electrons for HC_3N and He, H_2 and electrons for CH_3CN, and only electrons otherwise, assuming an electron fraction $n(e)/n(H_2) = 3\times10^{-4}$. The transition observed in this work is shown in red, dashed lines.

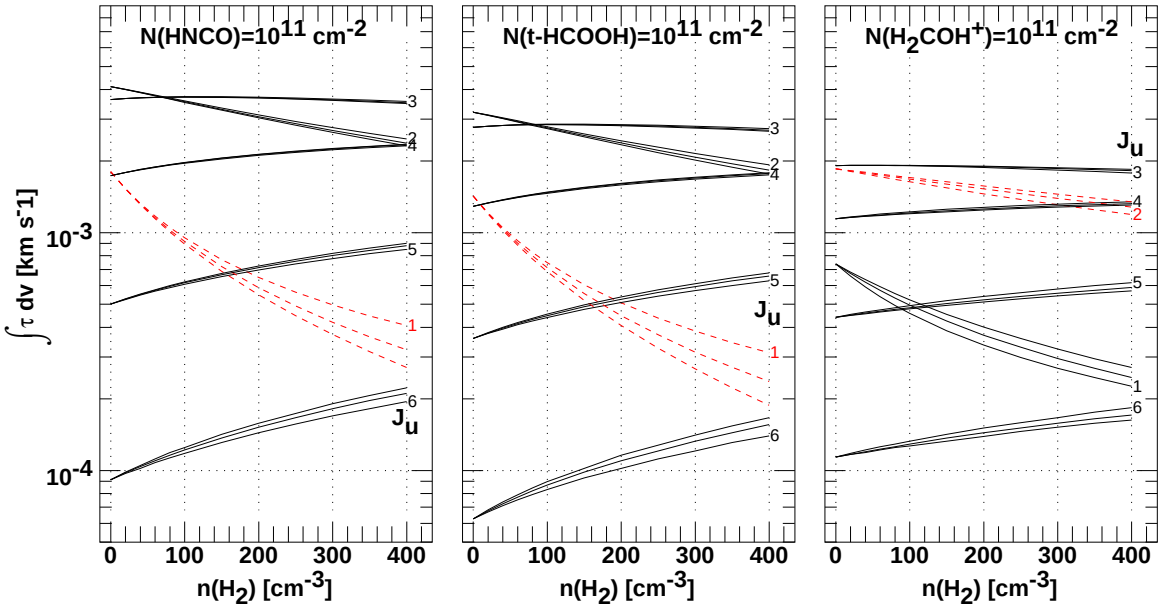

Figure A2. Integrated optical depth for rotational transitions of three oxygen-bearing molecules observed in the course of this work, assuming a column density of 10^{11} cm^{-2} in each case. The plots show the integrated optical depth of transitions whose upper-level quantum number is shown at the right of each series of three curves. The three curves correspond to calculations at kinetic temperatures of 20, 40 and 60 K. The calculations include electron excitation only, assuming an electron fraction n(e)/n(H_2) = 3×10^{-4}. The transition observed in this work is shown in red, dashed lines.

Visser, R., van Dishoeck, E. F., & Black, J. H. 2009, A&A, 503, 323
Watson, W. D., Anicich, V. G., & Huntress, W. T., J. 1976, ApJ, 205, L165
Weselak, T., Galazutdinov, G., Beletsky, Y., & Krełowski, J. 2009, A&A, 499, 783
Weselak, T., Galazutdinov, G. A., Beletsky, Y., & Krełowski, J. 2010, Mon. Not. R. Astron. Soc., 402, 1991
Zuckerman, B., Ball, J. A., & Gottlieb, C. A. 1971, ApJ, 163, L41

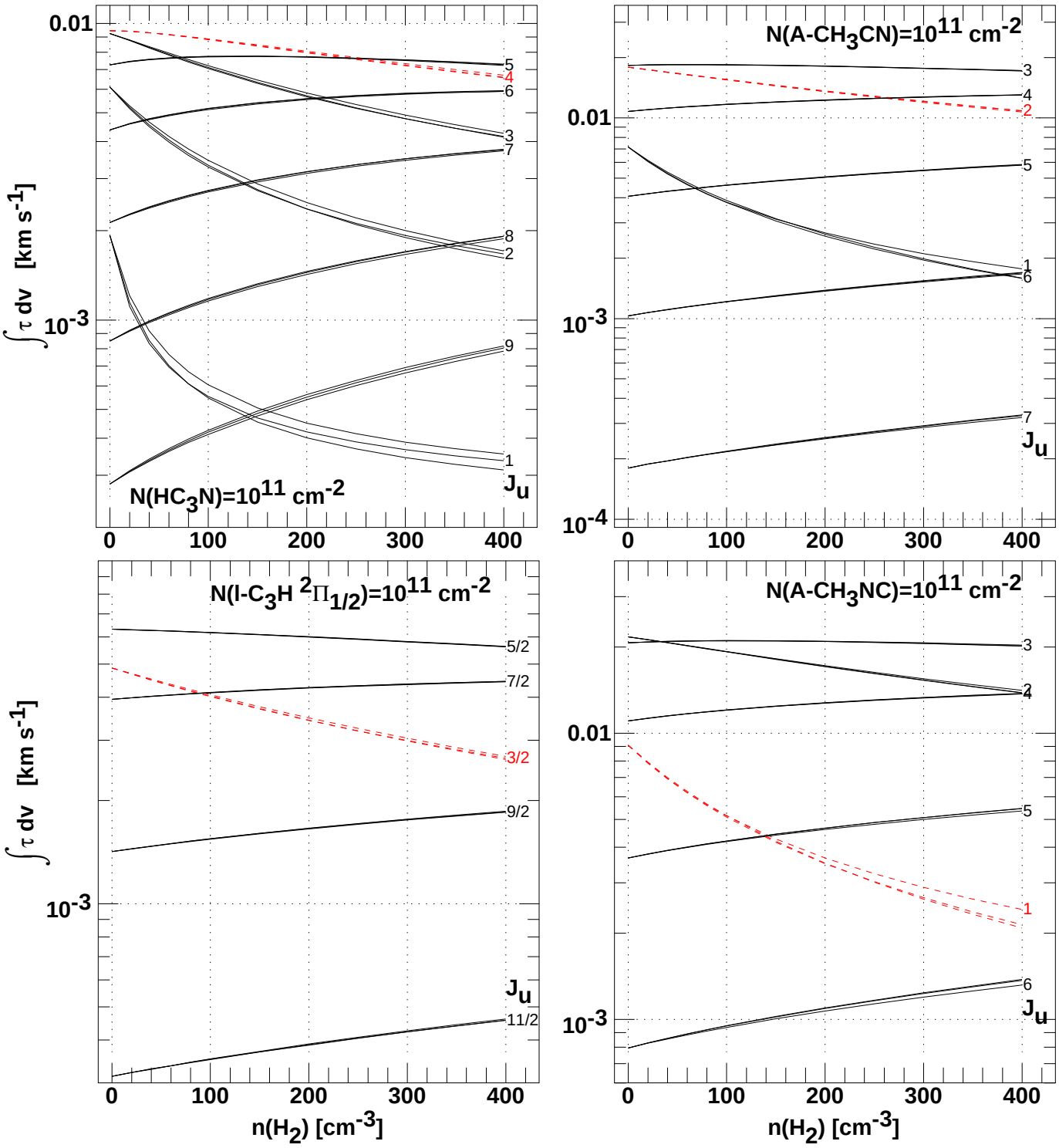
0.01
10-3
10-4
∫ τ dv [km s-1]
N(HC3N)=1011 cm-2
N(A-CH3CN)=1011 cm-2
N(l-C3H 2Π1/2)=1011 cm-2
N(A-CH3NC)=1011 cm-2
Ju
5
4
6
3
7
8
2
9
1
5/2
7/2
3/2
9/2
11/2
0
100
200
300
400
n(H2) [cm-3]

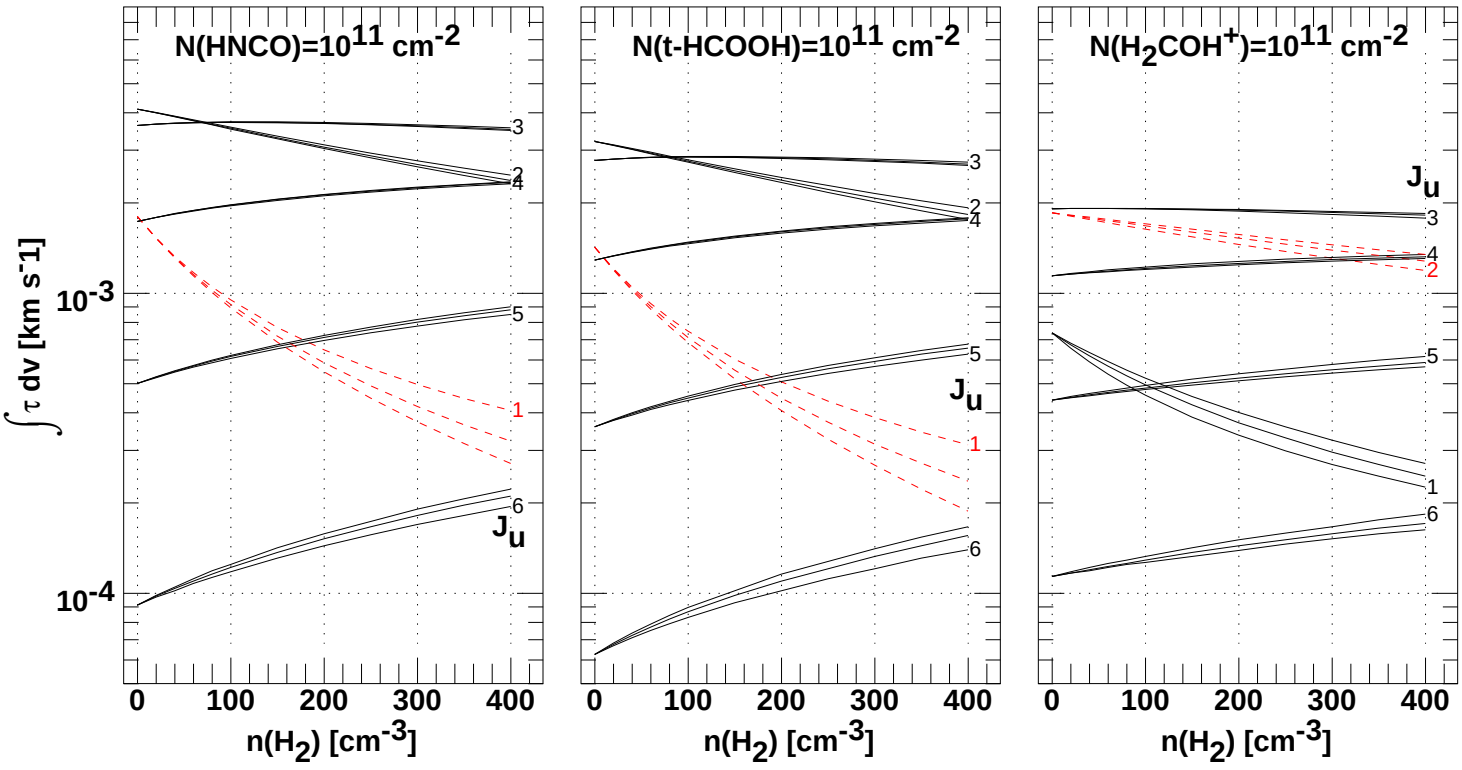
N(HNCO)=10^11 cm^-2
N(t-HCOOH)=10^11 cm^-2
N(H2COH+)=10^11 cm^-2
∫τ dv [km s^-1]
10^-3
10^-4
0
100
200
300
400
n(H2) [cm^-3]
Ju
1
2
3
4
5
6